Optical properties of Ge-rich Ge_{1−x}Si_{x} alloys: Compositional dependence of the lowest direct and indirect gaps

Chi Xu, J. D. Gallagher, C. L. Senaratne, J. Menéndez, and J. Kouvetakis

Phys. Rev. B **93**, 125206 — Published 9 March 2016

DOI: 10.1103/PhysRevB.93.125206

Optical properties of Ge-rich $Ge_{1-x}Si_x$ alloys: compositional dependence of the lowest direct and indirect gaps

Chi Xu[1], J.D. Gallagher[1], C.L. Senaratne[2], J. Menéndez[1], J. Kouvetakis[2]

[1]Department of Physics, Arizona State University, Tempe, AZ 85287-1504

[2]School of Molecular Sciences, Arizona State University, Tempe, AZ 85287-1604

Abstract

Ge-rich $Ge_{1-x}Si_x$ alloys have been investigated using spectroscopic ellipsometry and photoluminescence at room temperature. Special emphasis was placed on the compositional dependence of the lowest-energy interband transitions. For $x \leq 0.05$, a compositional range of particular interest for modern applications, we find $E_0 = 0.799(1)+3.214(45)x+0.080(44)x^2$ (in eV) for the lowest direct gap. The compositional dependence of the indirect gap is obtained from photoluminescence as $E_{ind} = 0.659(4)+1.18(17)x$ (in eV). We find no significant discrepancies between these results and extrapolations from measurements at higher Si concentrations. Such discrepancies had been suggested by recent work on $Ge_{1-x}Si_x$ films on Si. An accurate knowledge of the interband transition energies is an important requirement for the design of devices incorporating Ge-rich $Ge_{1-x}Si_x$ alloys and for the understanding of more complex systems, such as ternary $Ge_{1-x-y}Si_xSn_y$ alloys, in terms of its binary constituents.

I. INTRODUCTION

From the early days of semiconductor physics, the full miscibility of Si and Ge has made it possible to grow and characterize $Ge_{1-x}Si_x$ solid solutions over the entire compositional range $0 \leq x \leq 1$. The material has become a paradigm of a random alloy whose properties are well described within the simple picture of a virtual crystal.[1] The subsequent development of epitaxial growth techniques has enabled the applications that make $Ge_{1-x}Si_x$ an important component of the materials portfolio in modern semiconductor technology, and this has motivated additional studies of the electronic, transport, and optical properties of the alloy.[2,3] The epitaxial $Ge_{1-x}Si_x$ films that have received most of this attention are near the Si-rich end, for which the modest lattice mismatch with the preferred Si substrates makes it possible to grow thick pseudomorphic layers devoid of strain-relaxation defects.[4] However, recent renewed interest in using pure Ge in logical[5] and optical[6,7] devices suggest that Ge-rich $Ge_{1-x}Si_x$ alloys will find increasing applications as stressors and barrier layers in Ge-based devices. Moreover, understanding the properties of Sn-containing ternary alloys such as $Ge_{1-x-y}Si_xSn_y$,[8-10] which typically contain $x < 0.2$, requires a detailed knowledge of the underlying binary alloys, including Ge-rich $Ge_{1-x}Si_x$.

The possible optical applications of Ge and Ge-rich group-IV alloys are based on the proximity of E_0—the lowest direct transition at the center of the Brillouin zone (BZ)—to the fundamental band gap. However, very few studies are available on the compositional dependence of E_0 in $Ge_{1-x}Si_x$. This scarcity of results extends even to pure Si, for which E_0 overlaps in energy with much stronger absorption features, which make it undetectable at all but the lowest temperatures.[11] Almost 50 years ago, Kline, Pollak, and Cardona (KPC), published a study of E_0 in $Ge_{1-x}Si_x$ alloys (with $0.06 < x < 0.5$) based on electroreflectance measurements.[12] The compositional dependence was found to be very linear. This linearity was quantified by a recent fit of the KPC data using an expression of the form $E_0(x) = E_0^{\mathrm{Ge}}(1-x) + E_0^{\mathrm{Si}}x - b_0^{\mathrm{GeSi}}x(1-x)$, which gives a small bowing parameter $b_0^{\mathrm{GeSi}} = 0.21$ eV. (Ref. 13) Electroreflectance measurements in fully strained, single-crystalline $Ge_{1-x}Si_x$/Si films with $x > 0.7$ (Ref. 14) are also consistent with a small bowing parameter. However, more recent results on partially relaxed $Ge_{1-x}Si_x$/Si films with $x < 0.06$ show significant deviations from the E_0 energies predicted from the KPC compositional dependence combined with standard deformation potential theory.[15] The uncertainty regarding the value of E_0 in Ge-rich $Ge_{1-x}Si_x$ not only makes it very difficult to design optical devices based on these alloys, but also creates

serious obstacles to the study of new materials such as the ternary $Ge_{1-x-y}Si_xSn_y$ alloy. Given the two-dimensional compositional space of the ternaries, which makes it much more difficult to map compositional dependencies, it is essential to validate interpolation expressions for all relevant transitions, including E_0. A quadratic interpolation formula for the ternary involves the three binary alloy bowing parameters b_0^{GeSi}, b_0^{GeSn}, and b_0^{SiSn}.(Ref. 16) Since the bowing parameter b_0^{SiSn} for the binary $Si_{1-y}Sn_y$ alloy has not been determined experimentally, attempts have been made to extract b_0^{SiSn} from fits to the ternary alloy using the known bowing parameters b_0^{GeSi} and b_0^{GeSn} for $Ge_{1-x}Si_x$ and $Ge_{1-y}Sn_y$ alloys, respectively.[8,9,17] However, since all available $Ge_{1-x-y}Si_xSn_y$ samples are near the Ge-rich end, the leading contributions to the E_0 energy associated with each bowing parameter are of the form $b_0^{GeSi}x$, $b_0^{GeSn}y$, and $b_0^{SiSn}xy$, respectively. This means that any uncertainty Δb_0^{GeSi} translates into a much larger $\Delta b_0^{GeSi}/y$ uncertainty in b_0^{SiSn}. In other words, meaningful fits of b_0^{SiSn} in available ternary alloys require a very accurate knowledge of the bowing parameters in binary $Ge_{1-x}Si_x$ and $Ge_{1-y}Sn_y$ alloys. Ironically, while such accurate data are now available for the more exotic $Ge_{1-y}Sn_y$ (Ref. 18), the above-mentioned uncertainties in the case of $Ge_{1-x}Si_x$ represent the main bottleneck for further progress in this field.

In this paper, we present a new study of the optical properties of single-crystal Ge-rich $Ge_{1-x}Si_x$ alloys, with emphasis on the compositional dependence of E_0. We use spectroscopic ellipsometry to determine the E_0 edge using two alternative methods: the traditional approach which consists in fitting analytical critical point expressions to numerical derivatives of the dielectric function, and a method based on fitting the rising edge of the imaginary part of the dielectric function with realistic expressions that include excitonic effects. An additional approach to the spectroscopy of the E_0 transition in Ge-rich materials is room temperature photoluminescence (PL).[19-24] Emission from E_0 is very weak in bulk Ge crystals due to reabsorption,[25-27] but becomes the strongest feature in micron-thick films. Accordingly, we now extend these studies to $Ge_{1-x}Si_x$ alloys, where the increasing separation between E_0 and the lowest indirect transitions should lead to a weakening of the E_0 signal, a trend that is confirmed by our experimental data.

Our ellipsometric results are in very good agreement with the KPC data. We do not observe the anomalies reported in Ref. 15. The PL data shows emission peaks that can be associated to the E_0 gap and to the fundamental band gap E_{ind}, as seen in Ge , $Ge_{1-y}Sn_y$, and Ge_{1-}

$_{x-y}Si_xSn_y$ alloys.[26,28,29] An additional intermediate peak seems unique to $Ge_{1-x}Si_x$ alloys and its origin is unclear.

II. SAMPLE GROWTH AND CHARACTERIZATION

$Ge_{1-x}Si_x$ samples with $0 < x < 0.13$ were produced for this study on 4-inch Si(100) wafers in a Gas Source Molecular Epitaxy (GSME) chamber through reactions of Ge_4H_{10} and Si_4H_{10} at 380°C using mixtures with a Ge:Si molar ratio roughly half of the measured ratio in the resultant films. The film thicknesses ranged from 650 nm to 1740 nm. Upon completion of the growth, the wafers were subjected to an *in situ* anneal at 700°C for 3 minutes to improve the crystal quality of the epilayer. Once removed from the growth chamber, the samples were characterized by high resolution X-ray diffraction (XRD), and Rutherford backscattering (RBS) to determine crystallinity, composition, and thickness. The full width at half maximum (FWHM) of the (004) XRD reflection provided an initial test of sample quality. $Ge_{1-x}Si_x$ layers with $x \leq 0.05$ showed a FWHM as low as 0.05° even when grown directly onto the Si substrate. For films with $x > 0.05$, we found that their x-ray FWHM could be reduced if grown on Ge-buffered Si (Ref. 29) as opposed to directly on Si. Three samples with $x = 0.046$, 0.054, and 0.068 were grown on such Ge buffer layers. The thickness of the Ge buffer layers ranged from 600 nm to 880 nm.

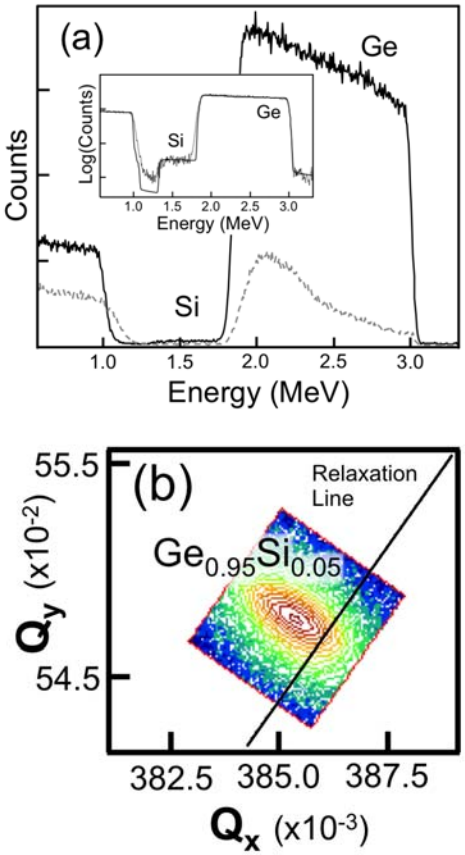

Figure 1 (a) 3.7 MeV RBS from a sample grown on Ge-buffered Si. The solid black line corresponds to the random mode and the dashed grey line corresponds to the channeling mode. Clear Ge and Si signals are seen from the top $Ge_{0.95}Si_{0.05}$ layer. The Ge (buffer) and $Ge_{0.95}Si_{0.05}$ thicknesses are measured to be 650 nm and 1600 nm, respectively. (b) 224 reciprocal space map of a $Ge_{0.950}Si_{0.050}$ alloy grown on Si(100). A biaxial tensile strain of 0.14% is measured from the peak position slightly above the cubic relaxation line.

Figure 1 (a) shows RBS spectra from a $Ge_{0.946}Si_{0.054}$ layer grown on Ge-buffered Si. The black (grey) line corresponds to the random (channeling) mode for an incident ion energy of 3.7 MeV. A high degree of channeling is observed

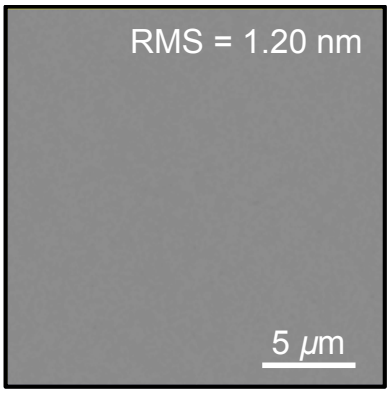

Figure 2 20 μm x 20 μm AFM image of a $Ge_{0.88}Si_{0.12}$ sample. Notice the absence of any Si-related pit defects.

across the entire sample thickness, demonstrating that the Ge buffer and $Ge_{0.95}Si_{0.05}$ epilayer are epitaxially aligned to the (001) orientation of the Si substrate. The low backscattering intensity of the channeled spectrum also corroborates the substitutional incorporation of Si atoms into the $Ge_{1-x}Si_x$ lattice. The inset shows the random spectrum on a logarithmic scale, highlighting the Si peak at the left side of the Ge peak. The solid line over these data represents the model fit to the spectrum. The Si profile is seen to be flat, indicating a uniform distribution of atoms across the layer.

The Si content of the films, crucial for the subsequent spectroscopic work, was derived from XRD (224) reciprocal space maps. An example is shown in Fig. 1(b) for a $Ge_{1-x}Si_x$ sample grown directly on Si. From such maps we determine the in-plane (a) and out-of-plane (c) lattice parameters. The relaxed lattice constant a_0 is then obtained from a and c using standard elasticity theory expressions, and the Si-concentration x is finally extracted from the known compositional dependence of a_0, including non-linear deviations from Vegard's law.[30] The Si film compositions obtained with this method are in excellent agreement with the values obtained directly from fitting RBS spectra. The X-ray measurements also make it possible to determine the level of strain, defined as $(a\text{-}a_0)/a_0$. This strain is tensile in most samples—due to the thermal expansivity mismatch with the Si-substrate—and quite modest in magnitude, never exceeding 0.2%. Nevertheless, strain corrections, as described below, were applied in all cases to extract relaxed values of the optical transition energies.

Figure 2 shows a 20 μm x 20 μm atomic force microscopy (AFM) image of a $Ge_{0.88}Si_{0.12}$ sample, illustrating a flat free surface devoid of pits or features projecting above the surface.[15] The average RMS roughness is ~ 1 nm irrespective of sample size and image dimensions. This value is typical of all films grown in this study using ultra-low temperature reactions of Ge_4H_{10} and Si_4H_{10}. The above results demonstrate that the samples are single-phase random alloys with high quality structural, compositional and morphological characteristics.

III. SPECTROSCOPIC ELLIPSOMETRY STUDIES

A) MEASUREMENT DETAILS AND DATA EXTRACTION

Ellipsometry measurements were carried out from 0.6 eV to 1.6 eV at a 0.005 eV steps and three incident angles of 65°, 70°, and 75° using a JA Woollam™ UV–VIS variable angle spectroscopic ellipsometer. The sample was modeled as a 4 or 5-layer structure, including the Si substrate, the Ge buffer layer (if present), a parameterized layer for the targeted $Ge_{1-x}Si_x$ film, a thin germanium oxide layer, and a surface roughness layer.

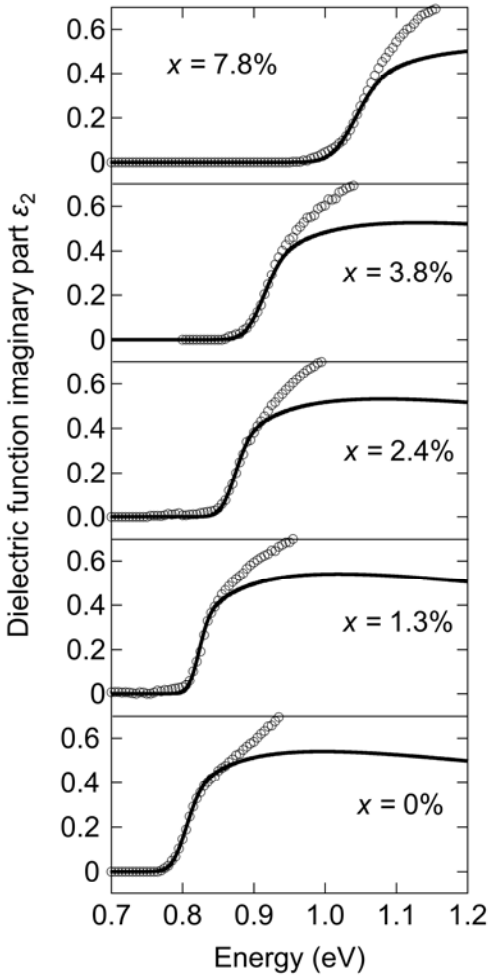

Figure 3 Imaginary part of the dielectric function for selected $Ge_{1-x}Si_x$ alloys. The empty circles represent the point-by-point fit to the ellipsometric data. The solid line was calculated on the basis of Eq. (2) and adjusted to the data to extract the E_0 band gap. The discrepancy between theory and experiment at higher energies is a result of assuming spherically symmetric parabolic bands and neglecting the contribution from the split-off band.

The complex dielectric function $\varepsilon_1 + i\varepsilon_2$ of the $Ge_{1-x}Si_x$ films was extracted from the ellipsometric data following a standard two-step procedure. In the first step, the known dielectric functions for the substrate and buffer layers were combined with a parametric model dielectric function for the $Ge_{1-x}Si_x$ layers.[31] The dielectric function parameters plus the thickness of all layers were then adjusted to obtain the best possible fit. In samples with no buffer layers, the adjusted $Ge_{1-x}Si_x$ thicknesses agreed within 2% with the RBS values. A similar agreement was obtained for the *total* Ge buffer plus $Ge_{1-x}Si_x$ thickness in samples grown on buffer layers. In these samples the individual layer thicknesses from the ellipsometry fits were within 10% of the RBS values.

In a second step, all layer thicknesses were frozen at the values determined in the first step, and the ellipsometric data were fit again at each energy point using the values of ε_1 and ε_2 for the $Ge_{1-x}Si_x$ layer as adjustable parameters, and the previous point's values as initial guess. This

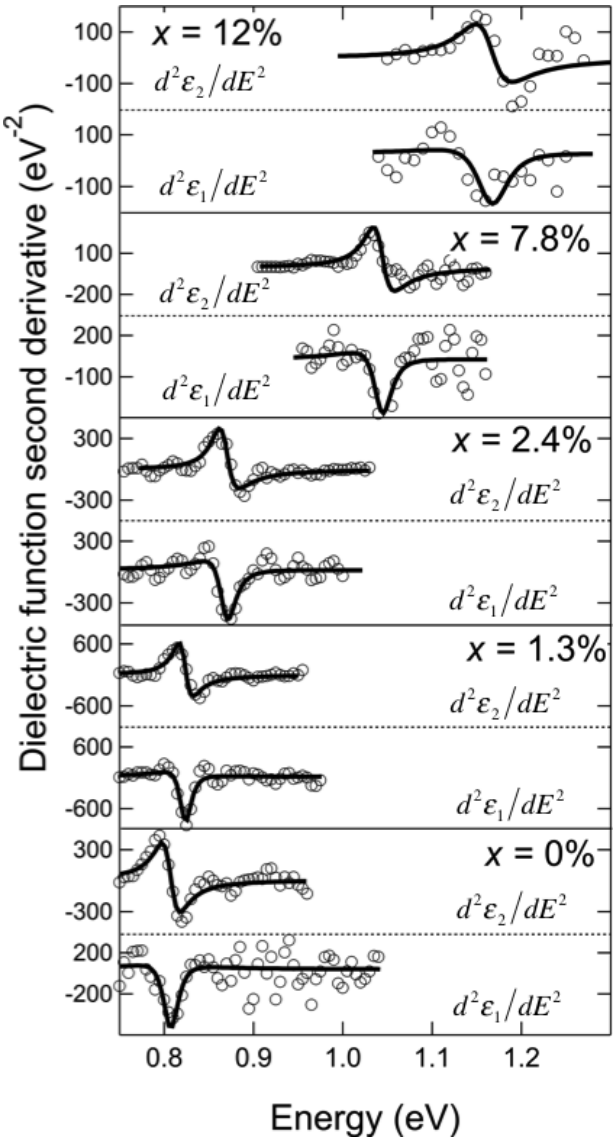

Figure 4 Numerical second derivatives of the real and imaginary parts of the dielectric function of selected $Ge_{1-x}Si_x$ samples. The solid lines are fits with Eq. (3).

procedure largely eliminates any possible bias introduced by specific parametric models with a pre-defined set of critical points. In addition, it does not impose Kramers-Kronig consistency between the real and imaginary parts, so that the verification of such consistency can be used as an additional control criterion for the quality of the fit. In general, the "point-by-point" dielectric functions obtained in the second iteration are found to be very close to the model dielectric functions of the first iteration, which are Kramers-Kronig consistent by construction. For the case of Ge-buffered samples we verified that our final point-by-point dielectric function remained essentially unchanged if we set the layer/buffer thickness ratio equal to the RBS value. We also obtained virtually identical results whether we used for the buffer layers bulk Ge optical constants or separately measured optical constants from standalone Ge buffer layers on Si.

The imaginary parts of the dielectric functions obtained from our point-by-point fits are shown for selected films in Fig. 3. Critical point energies are traditionally extracted from the experimental dielectric function by computing second or third numerical derivatives with respect to energies. These derivatives are particularly noisy when the imaginary part approaches zero, and therefore they must be combined with robust smoothing methods. We investigated different Savitzky-Golay smoothing-differentiation algorithms and found that an 11-point/4th-order polynomial filter reduces noise sufficiently to allow for critical point fits while introducing a

negligible distortion of the lineshapes. Second derivatives obtained with this approach are shown in Fig 4.

B) DETERMINATION OF E_0 ENERGIES

The textbook approach to extracting the E_0 energy from optical data is to fit a straight line to a plot of the *square* of ε_2. This is based on the observation that the E_0-contribution to the dielectric function is proportional to $(E\text{-}E_0)^{1/2}$. However, the exact expression, assuming parabolic bands, no broadening, and free electron-hole pairs, is given by the sum of two terms of the form[32]

$$\varepsilon_2(E) = \left(\frac{4\sqrt{2}e^2P^2}{3m^2\hbar E^2} \right) \mu_{eh}^{3/2} \left(E - E_0 \right)^{1/2} , \qquad (1)$$

where e and m are the free-electron charge and mass, μ_{eh} is the reduced effective mass of the electron-hole pair, and P the momentum matrix element. The two terms to be added correspond to the two degenerate light- and heavy-hole bands at the top of the valence band, which give different values of the reduced effective mass. A calculation with parameters appropriate for Ge (Ref. 33) and broadened to match room-temperature ellipsometric measurements gives the dot-dashed curve in Fig. 5, which deviates from a straight line due to the E^2 factor in the denominator of Eq. (1). Even more importantly, Eq. (1) is in poor agreement with experimental data for Ge, as demonstrated previously.[33] The disagreement can be partially concealed by introducing a multiplicative amplitude pre-factor in Eq. (1), but this is physically unsatisfactory because all prefactors in the equation are well known experimentally. Much better agreement with experiment can be obtained by introducing excitonic effects.

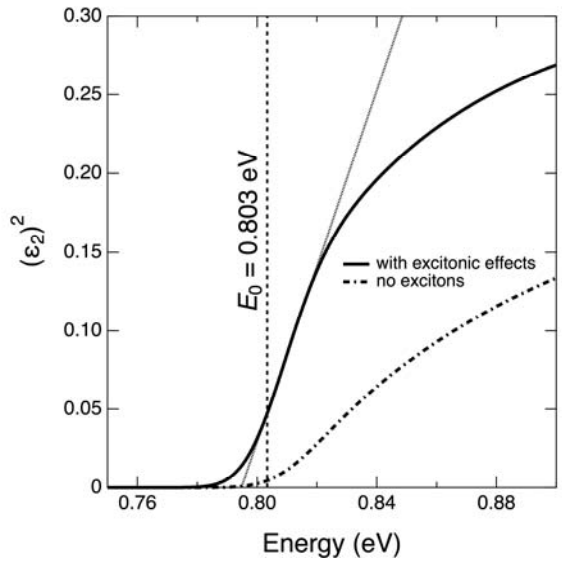

Figure 5 Calculated square of the imaginary part of the dielectric function at 300 K near the E_0 gap of Ge, using experimental values for the broadening parameter. The E_0 value in the simulation is indicated by the vertical dashed line. The dash-dotted line corresponds to the free electron-hole pair expression in Eq. (1). It deviates from a straight line due to the E^2 factor in the denominator. The solid line shows a calculation of ε_2^2 that includes excitonic effects following Eq. (2). This curve does show a region that can be approximated as a straight line, but the usual extrapolation to $\varepsilon_2 = 0$ gives a band gap value smaller than the actual E_0.

For a single pair of parabolic valence-conduction bands, the imaginary part of the excitonic dielectric function is given by

$$\varepsilon_2(E) = \varepsilon_{2x}(E) + \varepsilon_{2f}(E)S(E) \ , \tag{2}$$

where ε_{2x} is the below-band gap contribution from bound excitons, ε_{2f} is the dielectric function for free-electron hole pairs, given by Eq. (1), and $S(E)$ is the so-called Sommerfeld enhancement factor for states in the continuum. Analytical expressions for ε_{2x} and $S(E)$ appear in many textbooks and are also given in Ref. 33, where it was shown that Eq. (2) leads to very good agreement with experiment, both in terms of lineshape and absolute value. The square of the Ge ε_2 calculated on the basis of Eq. (2) is shown in Fig. 5 as a solid line. Notice that no sharp excitonic peak is predicted at room temperature, but there is a substantial excitonic enhancement combined with a dramatic change of the overall lineshape with respect to the free-electron hole case. Interestingly, the excitonic curve shows a region that can be approximated as a straight line, which may be the fortuitous reason why the "straight-line method" remains popular in spite of its weak theoretical justification on the basis of Eq. (1). However, such strain line (shown in Fig. 5 as a thin dotted line) extrapolates to $\varepsilon_2 = 0$ at $E = 0.795$ eV, which is 8 meV below the actual E_0 gap in the simulation. A systematic error of this magnitude may be tolerable in many circumstances, but it can be easily eliminated by performing an actual fit of the rising edge of the imaginary part of the dielectric function using an expression based on Eq. (2). This was our method of choice, and we show examples of the fits in Fig. 3.

For our fits with Eq. (2) we find that Gaussian broadening is in better agreement with the data, even for pure Ge. The adjustable parameters of the fit are then the width of the broadening function and the band gap E_0. The momentum matrix elements and effective masses were calculated as in Ref. 33, and the effect of the residual strain was fully included using deformation potential theory with hydrostatic and shear deformation potentials a = -9.47 eV from Goñi *et al*. (Ref. 34) and b = 1.88 eV from Liu *et al*. (Ref. 35) , as critically reviewed in Refs. 29 and 36. Notice that no sharp excitonic peak is observed in ε_2 at room temperature, but, as indicated above, excitonic effects are critical to match the absolute value of ε_2 to the experimental data without any additional "amplitude" parameter. The high-energy deviations between the calculated and observed dielectric function are expected, since the assumed isotropic parabolic dispersion ceases to be a good approximation about 50 meV above the E_0 gap. The values of E_0 obtained by our method are shown as black squares in Fig. 6.

The most common approach for extracting band gap energies from ellipsometric data, as indicated above, is to enhance the critical point singularities by computing derivatives of the dielectric function. To use this method, we fit the numerical second derivatives of the real and imaginary parts of the dielectric function with an expression of the form[13]

$$\frac{d^2\varepsilon}{dE^2} = \frac{Ae^{i\Phi}}{\left(E - E_0 + i\Gamma\right)^{3/2}} \quad , \tag{3}$$

with A, Φ, Γ, and E_0 as adjustable parameters. Eq. (3) corresponds to free electron-hole pairs, except that the phase angle Φ is taken as an adjustable parameter to mimic excitonic effects. An additional, more subtle reason for the need of an adjustable phase factor is the fact that the addition of $-i\Gamma$ to the energy gap is not a fully consistent way to treat broadening, as pointed out by Kim *et al*.(Ref. 37) The convolution of the calculated dielectric function with a broadening function—as applied to the analysis of the data in Fig. 3—is not fully consistent either. However, while the precise form in which broadening is introduced is relatively unimportant in fits of ε_2, it becomes critical for its second derivative $d^2\varepsilon/dE^2$, and therefore the parameter Φ corrects, in a phenomenological way, for some of the lineshape deviations caused by an approximate treatment of broadening. Theoretical expressions that treat broadening rigorously have been given by Kim *et al*.(Ref. 37), but the results do not lead to analytical forms that can be easily used to fit experimental data.

Since our samples present some residual amounts of strain, ranging from -0.07% (compressive) to 0.2% (tensile), fits with the oscillator in Eq. (3) do not give the value of E_0 corresponding to relaxed alloys. To correct for this deficiency, the data should in principle be fit with two such oscillators, one for the light-hole transition and one for the heavy-hole transition, shifted from E_0 following deformation potential theory. An alternative approach, which we have utilized to minimize the number of initial fit parameters, is to fit the data with the single oscillator represented by Eq. (3) and then adjust the resulting fit lineshape with two oscillators, separated by a fixed energy (ranging from -4 meV to 14 meV for the above values of strain) given by deformation potential theory. In this second fit, only E_0 and the value of Γ are allowed to be further adjusted. The phase angle is kept unchanged and the amplitudes A_{lh}, A_{hh} for the light- and heavy-hole transitions are simply taken, in the spirit of Eq. (1), as $A_{lh} = A\left(\frac{\mu_{lh}^{3/2}}{\mu_{lh}^{3/2}+\mu_{hh}^{3/2}}\right)$ and

$A_{hh} = A\left(\frac{\mu_{hh}^{3/2}}{\mu_{lh}^{3/2}+\mu_{hh}^{3/2}}\right)$, where A is the amplitude from the one-transition fit in Eq. (3). Values of E_0 extracted from these fits are shown in Fig. 6 as white circles.

The agreement between the E_0 values determined following the two methods described above is excellent, so that they will be combined for the analysis of the compositional dependence of E_0. Notice, however, that the second-derivative analysis is less robust, and for some samples the noise is simply too large to obtain meaningful fits.

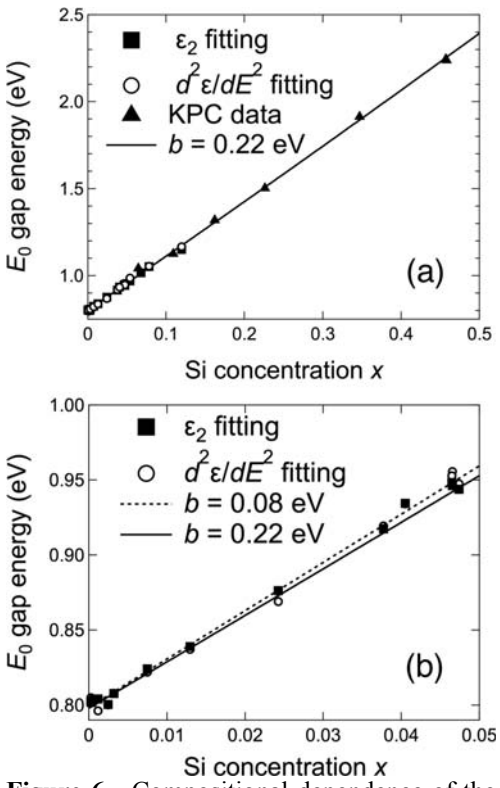

Figure 6 Compositional dependence of the E_0 transition energy in $Ge_{1-x}Si_x$ alloys (circles and squares). Panel (a) combines the data with previous measurements of this transition by KPC (Ref. 12). The solid line is a fit of the data using E_0^{Si} = 4.093 eV, which yields b_0^{GeSi} =0.22(2) eV and E_0^{Ge} = 0.803(2) eV. Panel (b) shows a detail of the $x \leq 0.05$ range. A fit restricted to this range gives b_0^{GeSi} =0.08 eV and is shown as a dashed line. Typical experimental error bars are about 2 meV, roughly the marker size.

C) COMPOSITIONAL DEPENDENCE OF E_0

The compositional dependence of the E_0 values in Fig. 6 is clearly very linear over the Si-concentration in the figure. A straight-line fit yields E_0 = 0.800(1) + 3.157(14) x (in eV). The extrapolation of this expression to x = 1 gives E_0 = 3.96 eV. Unfortunately, this cannot be directly compared with measurements in pure Si because the only experimental value available was obtained at 4.2 K by Aspnes *et al*., who found E_0 = 4.185 eV. (Ref. 11) Lautenschlager *et al*. have calculated the temperature dependence of all important transitions in Si and found very good agreement with all available experimental data.[38] If we combine the experimental value of E_0 at 4.2 K (Ref. 11) with the theoretical temperature dependence, we estimate a value E_0 = 4.093 eV for Si at room temperature. This would imply a modest non-linearity in the compositional dependence of E_0. As indicated in the introduction, deviations from linearity in the compositional dependence of transition energies are accounted to lowest order by introducing a bowing parameter b_0^{GeSi}. When the KPC data was fit using E_0^{Si} =4.093 eV, a value b_0^{GeSi} = 0.21 eV was

obtained.[13] A new fit that combines the KPC data with our results, shown as a solid line in Fig. 6, gives $E_0^{Ge} = 0.803(2)$ eV and essentially the same bowing parameter $b_0^{GeSi} = 0.22(2)$ eV. Thus our data are consistent with the KPC measurements. For very low concentrations $x \leq 0.05$, which are of particular interest in modern applications, the fit gives $E_0^{Ge} = 0.7986(12)$ eV, $b_0^{GeSi} = 0.080(44)$ eV, essentially a linear dependence. This is shown as a dashed line in Fig 6(b). The difference in bowing parameters between the $x \leq 0.5$ and $x \leq 0.05$ fits suggests that b_0^{GeSi} is not a constant but a function of composition. A bowing parameter of the form $b_0 = b_0^{(0)} + b_0^{(1)} y$ has already been found necessary to describe the compositional dependence of E_0 in $Ge_{1-y}Sn_y$ (Ref. 18) and similar expressions have been used for III-V alloy systems.[39,40] However, in the case of $Ge_{1-x}Si_x$ the bowing parameter is very small, making it very difficult to carry out a fit using $b_0^{GeSi} = b_0^{(0),\,GeSi} + b_0^{(1),\,GeSi} x$. The values of $b_0^{(0),\,GeSi}$ and $b_0^{(1),\,GeSi}$ obtained from such fits are not well converged and vary dramatically if single points are removed from the fit. This is understandable in view of the small difference between the $b_0^{GeSi} = 0.21$ eV and $b_0^{GeSi} = 0.080$ eV curves in Fig. 6(b).

IV. PHOTOLUMINESCENCE STUDIES

A) MEASUREMENT DETAILS AND DATA EXTRACTION

PL experiments were conducted at room temperature. The samples were excited with a cw-980 nm laser focused to a ~20 μm spot with an average power of 200 mW incident on the sample surface. The emitted light from the sample was collected with a Horiba 140 mm f/3.9 Czerny-Turner micro-HR^{TM} spectrometer and detected by an InGaAs photodiode cooled with liquid nitrogen. In order to optimize the signal-to-noise ratio, a lock-in detection technique is applied via an optical chopper—coupled to the amplifier readout—that modulated the incident laser beam at 191 Hz. For samples with $x < 0.02$ a 1400 nm long pass filter was inserted between the light emitted from the sample and the spectrometer entrance slit to block possible PL from the Si substrate and second-order grating diffraction peaks from the laser. For samples with $x > 0.02$, a 1064 nm long pass filter was used instead, so that the PL light from the sample would not be attenuated.

Typical PL spectra of $Ge_{1-x}Si_x$ alloys are shown in Fig. 7. PL studies of these alloys are usually carried out at low temperatures, for which sharp features associated with band edge excitons and

phonon replicas are clearly observed.[41] For the spectroscopy of the E_0 transition, however, room temperature conditions are needed to populate the Γ-valley in the conduction band. In Ge- and $Ge_{1-y}Sn_y$ thin films, these conditions lead to the observation of a dominant peak, assigned to the E_0 transition, and a weaker, low-energy peak assigned to the indirect transition E_{ind} between the L-valley in the conduction band and the top of the valence band at the Γ-point of the BZ. In $Ge_{1-x}Si_x$ alloys, on the other hand, we observe a three-peak structure. By comparison with pure-Ge films, we assign the high-energy peak to E_0 and the low-energy peak to E_{ind}. Following the discussion in Ref. 29, we fit the E_0 peak with an exponentially modified Gaussian (EMG) profile and the E_{ind} peak with a Gaussian. The extra peak, labeled E_P in Fig. 7, is also modeled as a Gaussian. The corresponding gap energies are extracted by following the procedure described in Ref. 29. Briefly, the EMG component is fit with a theoretical expression for spontaneous emission from the E_0 gap based on a generalized van Roosbroeck–Shockley formula for which we compute the absorption coefficient using the same model as in Eq. (2). The quasi-Fermi levels required for the calculation are evaluated as a function of the photoexcited charge density by including the L-, Γ, and Δ-valleys in the conduction band, and the light-heavy hole manifold in the valence band. The effect of strain is built into the absorption coefficient expressions using deformation potential theory. The values of E_{ind} are obtained from the low-energy Gaussian component using a correction adjusted to pure Ge, as discussed in Ref. 29.

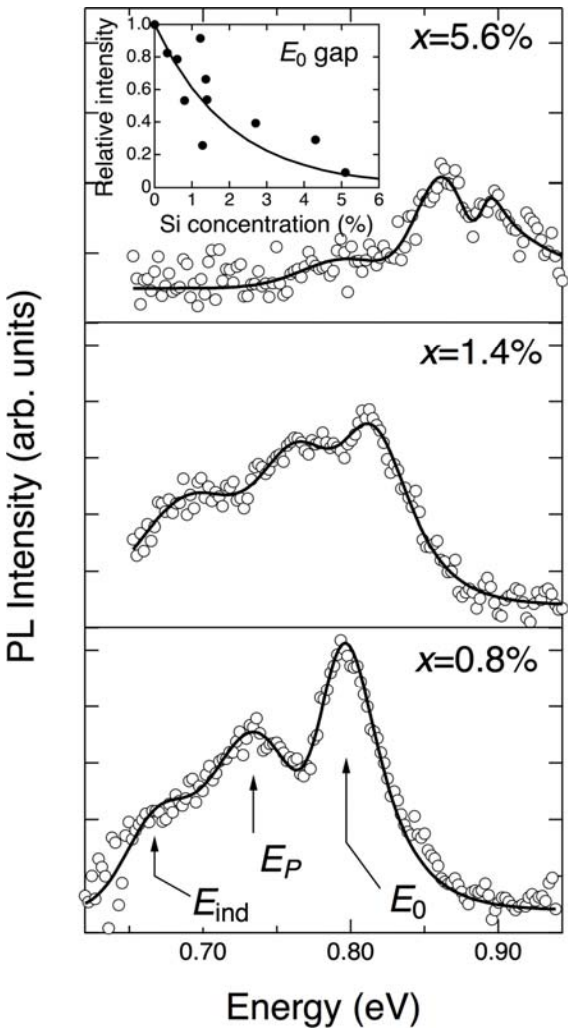

Figure 7 Representative room temperature PL spectra for selected $Ge_{1-x}Si_x$ samples. The inset in the top panel shows a comparison between measured and calculated integrated intensities (normalized to unity for pure Ge)

B) COMPARISON WITH ELLIPSOMETRY RESULTS

The E_0 values obtained from the PL data are

plotted in Fig. 8 and compared with the best fit to the ellipsometry data (dotted curve in Fig 6(b)). The agreement is quite good, but we notice that the energies obtained from the PL experiments are somewhat downshifted with respect to the ellipsometry values, particularly for the highest Si concentrations. A downshift of the PL signal with respect to the absorption edge (Stokes shift) is quite common in semiconductors. However, we cannot confirm this Stokes shift in our samples due to the presence of the E_P feature, which partially overlaps with the E_0 signal and could systematically shift the EMG fit. This is further complicated by the dramatic reduction in E_0 signal intensity as a function of the Si concentration. The reason behind this reduction is the increased separation between the Γ- and *L* minima in the conduction band, which reduces exponentially the population of the Γ-minimum. We have used our Roosbroeck–Shockley calculation to estimate the effect of the Si-concentration on the PL integrated intensity, and the calculation is compared with experimental data in the Fig. 7 inset. Good agreement is obtained, which indirectly supports our assignment of the leading peak to the E_0 transition. The order-of-magnitude reduction in PL intensity at the highest Si concentrations introduces larger errors in the determination of E_0, which could further contribute to the apparent discrepancy with the ellipsometry data.

The values of E_{ind} obtained from our PL lineshape analysis are also shown in Fig. 8. A linear fit gives $E_{\text{ind}} = 0.659(4)+1.18(17)x$ (in eV). This is in good agreement with the low-temperature PL measurements of Weber and Alonso, (Ref. 41) who find a linear coefficient of 1.27 eV.

A first candidate for the additional peak E_P observed in Fig. 7 is emission from the Δ-valley along the (100) direction of the BZ, which becomes the fundamental band gap for $x > 0.15$. By extrapolating low temperature PL measurements in samples with $x > 0.15$, the Δ-valley in pure Ge is predicted to be $\Delta E_{L\text{-}\Delta} = 0.19$ eV above the absolute minimum of the

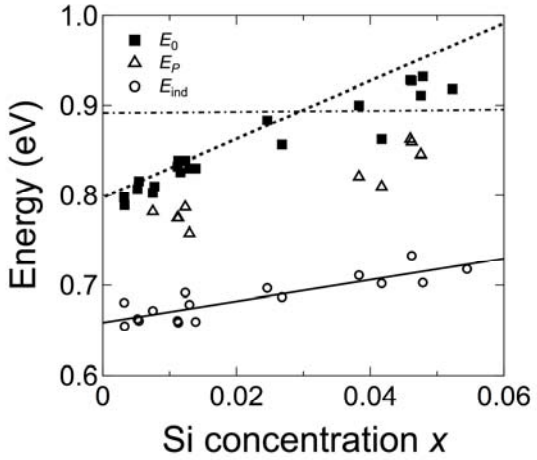

Figure 8. The E_0 and E_{ind} values extracted from the PL data are shown as black squares and empty circles, respectively. The peak energies for the E_P features shown in Fig. 7 are summarized as empty triangles. The solid line is a linear fit to the compositional dependence of E_{ind}. The dashed line is our best fit to the E_0 values obtained from ellipsometry. The dash-dotted line is the calculated peak energy for emission from the Δ-valley.

conduction band at the L point of the BZ.[41] This should be compared with a value $\Delta E_{L\text{-}\Delta} = 0.21$ eV obtained by Ahmad and Adams from electrical transport measurements,[42] and $\Delta E_{L\text{-}\Delta} = 0.22$ eV from an analysis of the broadening of the direct gap excitonic absorption under pressure.[43] Thus the Δ-minimum lies about 70 meV above the Γ-minimum in pure Ge, and this difference becomes smaller and eventually reverses sign in $Ge_{1-x}Si_x$ alloys. But even in the case of pure Ge, the population of Δ-valley under photoexcitation is calculated to be one order of magnitude higher than that of the Γ-valley, due to its much higher density of states. To compute the peak energy for possible emission from the Δ-valley we use the expression

$$I \propto \left[m_v^{3/2} m_\perp \left(2m_\parallel\right)^{1/2} \right] \times \left\{ \left(n_\Omega + 1\right) \exp\left[\frac{-\left(E+\hbar\Omega-\Delta F\right)}{k_\beta T}\right] E\left(E+\hbar\Omega-E_\Delta\right)^2 + n_\Omega \exp\left[\frac{-\left(E-\hbar\Omega-\Delta F\right)}{k_\beta T}\right] E\left(E-\hbar\Omega-E_\Delta\right)^2 \right\} \quad (4)$$

where E is the emitted photon energy, m_v is the effective hole mass, $m_\parallel$ and $m_\perp$ are the longitudinal and transverse effective masses at the Δ-valley, Ω a phonon frequency, E_Δ the Δ-valley minimum energy with respect to the top of the valence band, and ΔF the separation between quasi-Fermi levels in the conduction band. Combining the above result $\Delta E_{L\text{-}\Delta} = 0.21$ eV with the compositional dependence of the E_Δ energy measured by Weber and Alonso, we obtain at room temperature $E_\Delta = 0.874 + 0.046x + 0.206x^2$ (in eV). The maxima of the emission profiles computed by inserting this expression in Eq. (4) with a phonon energy $\hbar\Omega = 34.5$ meV (corresponding to a Ge-Ge like optical vibration) are shown as a dash-dotted line in Fig. 8, and we see that the calculated values not only exceed the observed E_P energies by a considerable amount but fail to account for the compositional dependence of E_P. Our calculation assumes fully relaxed layers, but if we incorporate strain effects (including the splitting of the 6 degenerate Δ-valleys into 4+2 manifolds, which never exceeds 30 meV), the predicted peak energies remain almost unchanged. Alternatively, one might assume that the dominant contribution arises from a Si-Ge like vibration with $\hbar\Omega \sim 50$ meV. This would slightly lower the dotted line in Fig. 8, but would not change its compositional dependence. Thus it seems unlikely that the E_P emission arises from the Δ-valley contribution.

Since the E_P energy seems to be tracking the E_0 energy, an alternative explanation for the E_P emission might be related to the splitting between light and heavy holes, but as indicated above this splitting is at most 14 meV in our samples, much less than the observed separation of

~60 meV between the E_P and E_0 features. In fact, our modeling of the E_0 transition does incorporate the light- heavy-hole splitting, and we do not predict the observation of two distinct peaks for typical values of the broadening parameter. It should also be pointed out that biaxial strain on the (001) plane does not split the minimum of the conduction band at the *L*-point of the Brillouin zone, and therefore the appearance of E_P cannot be related to splittings of the *L*-valleys. On the other hand, the average energy separation of 60 meV between E_0 and E_P corresponds to Si-Si-like phonon energies in $Ge_{1-x}Si_x$, raisng the possibility of an interpretation of E_P in terms of a phonon-assisted direct transition. However, such a phonon-assisted transition would be expected to be much weaker than the allowed no-phonon direct gap transition, whereas the E_P feature has an intensity comparable with the E_0 transition. Moreover, it is hard to see why Si-Si vibrations would make such a prominent contribution at Si-concentrations where there are very few Si-Si bonds in our samples. Yet another explanation might involve the existence of Si-depleted regions in the samples, for example at the interface with the buffer/substrate or near the surface. These regions, if they exist, should occupy a negligible volume, because they are not apparent in the RBS measurements (Fig. 1) and they do not affect the ellipsometry measurements. Still, their contribution might be enhanced in emission because E_0 in those regions would have a lower value. However, this explanation would imply that all E_P peak energies should be higher than that of pure Ge, and this is not the case experimentally, as clearly seen in Fig 8.

Finally, the fact that E_P seems to track E_0 suggest an alternative explanation in terms of an acceptor level above the valence band maximum. Common shallow acceptors with binding energies close to 11 meV can be ruled out, but a defect level associated with epitaxial growth could have a binding energy closer to 60 meV. Such defects might be present even in pure Ge or GeSn layers on Si, but their emission would not be clearly observable in these systems because their E_0 emission is much stronger than in $Ge_{1-x}Si_x$. Emission studies on *n*-type doped $Ge_{1-x}Si_x$ layers should help investigate this possibility in depth.

CONCLUSION

In summary, we have carried out a detailed study of the optical properties of Ge-rich $Ge_{1-x}Si_x$ alloys. We find that at very low Si concentrations $x < 0.05$ the compositional dependence of the

E_0 gap is essentially linear when using the end point E_0^{Si} =4.093 eV for pure Si at room temperature. Our data are consistent within error with previous measurements by Kline, Pollak, and Cardona on samples with higher concentrations approaching x = 0.5. The two sets of data, combined, give a bowing parameter b_0^{GeSi} = 0.22 eV using the above value for E_0^{Si}. Our work demonstrates that the direct gap E_0 in Ge-rich $Ge_{1-x}Si_x$ can be observed in room-temperature photoluminescence experiments, as shown earlier for Ge, $Ge_{1-y}Sn_y$, and $Ge_{1-x-y}Si_xSn_y$ thin films. The photoluminescence experiments also show that the compositional dependence of the Ge-like indirect gap E_{ind} at room temperature is the same, within error, as the dependence measured earlier at low temperature. The accurate determination of the compositional dependence of E_0 and E_{ind} will contribute to the design of optical devices including $Ge_{1-x}Si_x$ components and to the understanding of more complex systems, such as ternary $Ge_{1-x-y}Si_xSn_y$ alloys, in terms of its binary constituents.

ACKNOWLEDGEMENTS

This work was supported by the Air Force Office of Scientific Research under contracts DOD AFOSR FA9550-12-1-0208 and AFOSR FA9550-13-1-0022.

REFERENCES

[1] S. Krishnamurthy, A. Sher, and A. B. Chen, Phys. Rev. B **33** (2), 1026 (1986).
[2] T. P. Pearsall, Prog. Quant. Electr. **18**, 97 (1994).
[3] D. J. Paul, Semicond. Sci. Technol. **19** (10), R75 (2004).
[4] E. Kasper and S. Heim, Applied Surface Science **224** (1-4), 3 (2004).
[5] C. Claeys and E. Simoen, *Germanium-Based Technologies: From Materials to Devices*. (Elsevier, Oxford, 2007), p.449.
[6] Y.-H. Kuo, Y. K. Lee, Y. Ge, S. Ren, J. E. Roth, T. I. Kamins, D. A. B. Miller, and J. S. Harris, Nature **437** (7063), 1334 (2005).
[7] J. Liu, X. Sun, R. Camacho-Aguilera, L. C. Kimerling, and J. Michel, Opt. Lett. **35** (5), 679 (2010).
[8] V. R. D'Costa, Y. Y. Fang, J. Tolle, J. Kouvetakis, and J. Menéndez, Thin Solid Films **518** (9), 2531 (2010).
[9] C. Xu, C. L. Senaratne, J. Kouvetakis, and J. Menéndez, Solid-State Electronics **110**, 76 (2015).
[10] P. Moontragoon, R. A. Soref, and Z. Ikonic, J. Appl. Phys. **112** (7), 073106 (2012).
[11] D. E. Aspnes and A. A. Studna, Solid State Commun. **11**, 1375 (1972).
[12] J. S. Kline, F. H. Pollak, and M. Cardona, Helvetica Physica Acta **41**, 968 (1968).
[13] V. R. D'Costa, C. S. Cook, A. G. Birdwell, C. L. Littler, M. Canonico, S. Zollner, J. Kouvetakis, and J. Menendez, Phys. Rev. B **73** (12), 125207 (2006).

[14] T. Ebner, K. Thonke, R. Sauer, F. Schaeffler, and H. J. Herzog, Phys. Rev. B **57** (24), 15448 (1998).
[15] D. D. Cannon, J. Liu, D. T. Danielson, S. Jongthammanurak, U. U. Enuha, K. Wada, J. Michel, and L. C. Kimerling, Appl. Phys. Lett. **91** (25), 252111 (2007).
[16] V. R. D'Costa, C. S. Cook, J. Menendez, J. Tolle, J. Kouvetakis, and S. Zollner, Solid State Commun. **138** (6), 309 (2006).
[17] V. R. D'Costa, Y. Y. Fang, J. Tolle, J. Kouvetakis, and J. Menendez, Phys. Rev. Lett. **102** (10), 107403 (2009).
[18] J. D. Gallagher, C. L. Senaratne, J. Kouvetakis, and J. Menéndez, Appl. Phys. Lett. **105** (14), 142102 (2014).
[19] X. Sun, J. Liu, L. C. Kimerling, and J. Michel, Appl. Phys. Lett. **95** (1), 011911 (2009).
[20] T. H. Cheng, C. Y. Ko, C. Y. Chen, K. L. Peng, G. L. Luo, C. W. Liu, and H. H. Tseng, Appl. Phys. Lett. **96** (9), 091105 (2010).
[21] J. Mathews, R. T. Beeler, J. Tolle, C. Xu, R. Roucka, J. Kouvetakis, and J. Menéndez, Appl. Phys. Lett. **97** (22), 221912 (2010).
[22] R. Chen, H. Lin, Y. Huo, C. Hitzman, T. I. Kamins, and J. S. Harris, Appl. Phys. Lett. **99** (18), 181125 (2011).
[23] L. Jiang, C. Xu, J. D. Gallagher, R. Favaro, T. Aoki, J. Menéndez, and J. Kouvetakis, Chemistry of Materials **26** (8), 2522 (2014).
[24] W. Du, S. A. Ghetmiri, B. R. Conley, A. Mosleh, A. Nazzal, R. A. Soref, G. Sun, J. Tolle, J. Margetis, H. A. Naseem, and S.-Q. Yu, Appl. Phys. Lett. **105** (5), 051104 (2014).
[25] J. R. Haynes, Phys. Rev. **98** (6), 1866 (1955).
[26] G. Grzybowski, R. Roucka, J. Mathews, L. Jiang, R. Beeler, J. Kouvetakis, and J. Menéndez, Phys. Rev. B **84** (20), 205307 (2011).
[27] T. Arguirov, M. Kittler, and N. V. Abrosimov, Journal of Physics: Conference Series **281**, 012021 (2011).
[28] J. D. Gallagher, C. Xu, L. Jiang, J. Kouvetakis, and J. Menéndez, Appl. Phys. Lett. **103** (20), 202104 (2013).
[29] L. Jiang, J. D. Gallagher, C. L. Senaratne, T. Aoki, J. Mathews, J. Kouvetakis, and J. Menéndez, Semicond. Sci. Technol. **29** (11), 115028 (2014).
[30] J. P. Dismukes, L. Ekstrom, and R. J. Paff, J. Phys. Chem. **68** (10), 3021 (1964).
[31] B. Johs, C. M. Herzinger, J. H. Dinan, A. Cornfeld, and J. D. Benson, Thin Solid Films **313-314**, 137 (1998).
[32] P. Y. Yu and M. Cardona, *Fundamentals of Semiconductors: Physics and Materials Properties*. (Springer-Verlag, Berlin, 1996).
[33] V. R. D'Costa, Y. Fang, J. Mathews, R. Roucka, J. Tolle, J. Menendez, and J. Kouvetakis, Semicond. Sci. Technol. **24** (11), 115006 (2009).
[34] A. R. Goñi, K. Syassen, and M. Cardona, Phys. Rev. B **39** (17), 12921 (1989).
[35] J. Liu, D. D. Cannon, K. Wada, Y. Ishikawa, D. T. Danielson, S. Jongthammanurak, J. Michel, and L. Kimerling, Phys. Rev. B **70** (15), 155309 (2004).
[36] J. Teherani, W. Chern, D. Antoniadis, J. Hoyt, L. Ruiz, C. Poweleit, and J. Menéndez, Phys. Rev. B **85** (20), 205308 (2012).
[37] C. C. Kim, J. W. Garland, H. Abad, and P. M. Raccah, Phys. Rev. B **45** (20), 11749 (1992).
[38] P. Lautenschlager, P. Allen, and M. Cardona, Phys. Rev. B **31** (4), 2163 (1985).

[39] D. E. Aspnes, S. M. Kelso, R. A. Logan, and R. Bhat, J. Appl. Phys. **60** (2), 754 (1986).
[40] V. Bellani, M. Geddo, G. Guizzetti, S. Franchi, and R. Magnanini, Phys. Rev. B **59** (19), 12272 (1999).
[41] J. Weber and M. I. Alonso, Phys. Rev. B **40** (8), 5683 (1989).
[42] C. N. Ahmad and A. R. Adams, Phys. Rev. B **34** (4), 2319 (1986).
[43] G. Li, A. Goñi, K. Syassen, and M. Cardona, Phys. Rev. B **49** (12), 8017 (1994).